CLOCK/BMAL1 interferes with segmentation clock oscillation in mouse embryonic organoids

Authors: Yasuhiro Umemura[a], Nobuya Koike[a], Yoshiki Tsuchiya[a], Hitomi Watanabe[b], Gen Kondoh[b], Ryoichiro Kageyama[c], and Kazuhiro Yagita[a,*].

Affiliations:

[a]Department of Physiology and Systems Bioscience, Kyoto Prefectural University of Medicine, Kawaramachi-Hirokoji, Kyoto 602-8566, Japan.

[b]Laboratory of Integrative Biological Science, Institute for Frontier Life and Medical Sciences, Kyoto University, Kyoto 606-8501, Japan.

[c]Laboratory of Growth Regulation System, Institute for Frontier Life and Medical Sciences, Kyoto University, Kyoto 606-8507, Japan.

*Correspondence to: Kazuhiro Yagita

Email: kyagita@koto.kpu-m.ac.jp

Phone: +81-75-251-5313

Fax: +81-75-241-1499

Abstract

In the mammalian developmental process, the segmentation clock and circadian clock appear sequentially in the embryo. However, there is no clear information about the biological significance of the mutual exclusiveness of these rhythms. Here we show that excess of the circadian components CLOCK/BMAL1 in mouse embryonic organoids, induced presomitic mesoderm and gastruloids, disrupts the *Hes7* ultradian rhythm and somitogenesis. RNA sequencing analysis showed that CLOCK/BMAL1 activates the signaling pathways regulating *Hes7*. After establishment of the circadian clock, the expression of endogenous *Hes7* and another segmentation clock gene, *Lfng*, tended to fluctuate with a circadian period, implying that the circadian clock potentially interferes with the segmentation clock. These results suggest that strict timing regulation of the emergence of circadian clock oscillation is essential for mammalian development.

Competing Interest Statement

The authors have declared no competing interest.

Main

The circadian clock is the cell-autonomous time-keeping system generating the temporal order of various physiological functions, which enables cells, organs, and systems to adapt to the cyclic environment of the rotating Earth (*1-5*). The core architecture of the circadian molecular clock consists of negative transcriptional/translational feedback loops (TTFLs) composed of a set of circadian clock genes, including *Bmal1*, *Clock*, *Period* (*Per1*, *2*, *3*), and *Cryptochrome* (*Cry1*, *2*), functioning under the control of E-box elements (*2, 6*). The kernel of TTFLs is composed of heterodimerized CLOCK/BMAL1 key transcriptional factors that positively regulate the circadian output genes, as well as *Per* and *Cry* genes via E-box. PERs and CRYs inhibit CLOCK/BMAL1 transcriptional activity, and the negative feedback loops between these genes generate oscillations of approximately 24 h.

In mammalian development, it has been demonstrated that early embryos and pluripotent stem cells have no apparent circadian molecular oscillations (*7-11*), whereas the innate circadian clock develops during ontogenesis and is established at a late developmental stage (*12-15*). Regarding the mechanisms regulating circadian clock development, using an *in vitro* model of embryonic stem cell (ESC) differentiation, it was shown that prolonged posttranscriptional mechanisms inhibiting CLOCK protein translation and nuclear translocation of PER proteins suppress the establishment of the circadian TTFL cycle, which may contribute to the delayed emergence of circadian oscillation in embryos (*16-18*).

In the early developmental stages, a segmented body plan is essential for an intact developmental process. Somitogenesis is related to another cell-autonomous oscillator, the segmentation clock, in the posterior presomitic mesoderm (PSM) (*19, 20*). The mouse segmentation clock is underlain by a negative feedback loop involving *Hes7* oscillation (*21, 22*).

HES7 is a key transcriptional factor that represses its own expression and oscillates through a negative feedback loop in a period of 2–3 h in mouse and 4–5 h in humans. The NOTCH, WNT, and fibroblast growth factor signaling pathways are involved in the regulation of the *Hes7* oscillator and its intercellular synchronization (*20*). In mammals, two different types of rhythm, the segmentation clock-derived ultradian rhythm and circadian rhythm, sequentially emerge during the developmental process. Interestingly, the temporal relationship between the segmentation clock and circadian clock appears to be mutually exclusive (**Fig. S1**); however, there is a lack of knowledge about the biological significance of the rhythm conversion during development.

Focusing on the functional interaction between these two biological clocks with different frequencies during the developmental process, intriguingly, one of the core circadian clock genes, *Per1*, is physically adjacent to an essential component of the segmentation clock, *Hes7*, in a genomic region conserved in higher vertebrates including mouse and humans (**Fig. 1A**). The *Per1* homolog *Per2* is also adjacent to the *Hes7* homolog *Hes6* in the genome. Since *Hes7* exhibits the essential characteristics of a segmentation clock (*23*), we have hypothesized that the transcriptional regulation of these genes may interfere with the adjacent gene expression rhythms. Therefore, we investigated the effect of the CLOCK/BMAL1-mediated activation of *Per1* transcription on the segmentation clock oscillation in induced presomitic mesoderm (iPSM), an *in vitro* recapitulating model of segmentation clock, using ESCs carrying the *Hes7*-promoter-driven luciferase reporter (*pHes7-luc*) (*24*) (**Fig. 1B**). Because the expression of CLOCK protein is suppressed posttranscriptionally in ESCs and early embryos (*17*), we established two ESC lines carrying the doxycycline (dox)-inducible *Clock* and *Bmal1* genes (**Fig. 1C**, **Fig. S2**). In iPSM differentiated from ESCs, the expression of both *Clock/Bmal1* mRNA and CLOCK/BMAL1 proteins was confirmed after the addition of dox (**Fig. 1D, E**), and we found

that overexpression of both *Clock* and *Bmal1* successfully activated the expression of core clock genes (**Fig. 1F**). As the dominant negative mutant of *Bmal1* (*Bmal1DN*) (*25*) co-expressed with *Clock* did not activate the *Per1/2* and *Cry1/2* genes, we concluded that CLOCK/BMAL1 specifically activated the expression of these clock genes via an E-box (**Fig. 1C–F**). We then examined the expression of genes in *Hes7*, which is proximal to *Per1*, and *Hes6*, which is proximal to *Per2* in the genome. The expression of *Clock/Bmal1* induced by dox in the iPSM induced significant upregulation of the expression of the *Hes7*, but not *Hes6*, gene (**Fig. 1G**). Similarly, we also observed the upregulation of *Hes7* expression by *Clock/Bmal1* induction in the undifferentiated ESCs (**Fig. S3A, B**). These results indicate that the circadian components CLOCK/BMAL1 also affect the segmentation clock gene *Hes7*, as well as *Per1*.

We next observed the segmentation clock oscillations in bioluminescence from *pHes7-luc* reporters using a photomultiplier tube device (PMT) and an EM-CCD camera in iPSM (**Fig. 2A**). We confirmed an oscillation of *Hes7*-promoter-driven bioluminescence with a period of approximately 2.5–3 h in control iPSM with or without dox using PMT and the EM-CCD camera (**Fig. 2B, C**). Traveling waves of *pHes7-luc* bioluminescence were observed, indicating that the segmentation clock oscillation in iPSM was successfully reproduced, consistent with a previous report (*24*). Using this iPSM-based segmentation clock system, we investigated the effect of *Clock/Bmal1* expression on *Hes7*-promoter-driven oscillation. The expression of *Clock/Bmal1* genes (Dox+) resulted in defects of the oscillation in *Hes7* promoter activity, whereas *pHes7-luc* bioluminescence continued to oscillate under Dox–conditions. Oscillation of the segmentation clock was observed even during the induction of *Clock/Bmal1DN* (**Fig. 2D**), indicating that the CLOCK/BMAL1-mediated mechanism disrupted the transcriptional oscillation of *Hes7*. A traveling wave of *Hes7* promoter activity disappeared with the expression of *Clock/Bmal1* (**Fig. 2E, F**), and dox-dependent arrest of *pHes7-luc*

traveling wave (**Fig. 2G, H**) clearly demonstrated the CLOCK/BMAL1-mediated interference with *Hes7*-driven segmentation clock oscillation in iPSM.

In addition, to explore the effect of CLOCK/BMAL1 expression on somitogenesis, we established the ESC-derived embryonic organoids, gastruloids, recapitulating an embryo-like organization, including somitogenesis-like process *in vitro* (*26*) (**Fig. 3A**). The *pHes7-luc* bioluminescence represented a traveling wave accompanied by the formation of segment-like structures with anteroposterior polarity, in which the gastruloids were stained as stripes of a somite marker, *Uncx4.1*, by *in situ* hybridization (**Fig. 3B–D**). Doxycycline treatment in control gastruloids derived from *pHes7-luc* ESCs induced no change in the *pHes7-luc* bioluminescence oscillation and somitogenesis-like process (**Fig. 3E–G**). Then, the dox-inducible *Clock/Bmal1* ESC line carrying *pHes7-luc* was differentiated *in vitro* into gastruloids and produced the somitogenesis-like process without dox (**Fig. 3H–J**). In contrast, the dox-dependent induction of *Clock/Bmal1* expression in the gastruloids interrupted the *pHes7-luc* oscillation and disrupted the somitogenesis-like structures (**Fig. 3K–M**). In gastruloids, the expression of both *Clock/Bmal1* mRNA at two hours after the addition of dox was confirmed (**Fig. S4**), which was consistent with the timing of dox treatment-induced interruption of the *Hes7* oscillation. These results suggest that the premature expression of the circadian components CLOCK/BMAL1 critically interferes with not only *Hes7* oscillation but also somitogenesis.

Next, to examine the perturbation mechanisms of the segmentation clock oscillation by the circadian components CLOCK/BMAL1, we analyzed the RNA sequencing (RNA-seq) data obtained from the total RNA of iPSM colonies. We extracted upregulated and downregulated differentially expressed genes (DEGs) after the induction of *Clock/Bma11* gene expression in iPSM colonies (**Fig. 4A**). A KEGG pathway enrichment analysis for the DEGs revealed

enrichment of the WNT, MAPK, and NOTCH signaling pathways, those of which have been shown to be regulatory mechanisms controlling the *Hes7* oscillation (*27*) (**Fig. 4B**). Almost other ranked pathways also included the WNT, MAPK, and NOTCH signaling pathway-related genes (**Fig. 4B**). Similarly, enrichment of the WNT, MAPK, and NOTCH signaling pathways by *Clock/Bmal1* induction was also observed in the undifferentiated ESCs (**Fig. S5A, B**). These findings indicate that the premature excess of CLOCK/BMAL1 activates the *Hes7*-related signaling pathways, which interferes with the feedback loop regulating *Hes7* oscillation. Intriguingly, in addition to *Hes7* gene expression, the expressions of *Aloxe3* and *Vamp2*, the other contiguous genes with *Per1*, were upregulated with the induction of *Clock/Bmal1* expression in iPSM and ESCs, and this result was confirmed by quantitative RT-PCR (qPCR) (**Fig. 4C–E**, **Fig. S5C–E**), suggesting that expression of CLOCK/BMAL1 affects *Hes7* expression also by indirect or ripple effects (*28*), in addition to the activation of the *Hes7* regulation network. These results suggest that the premature expression of the circadian components CLOCK/BMAL1 disrupts *Hes7* oscillation and somitogenesis by interfering with *Hes7*-related signaling pathways (**Fig. 4F**).

We next investigated the effect of circadian clock oscillation on the segmentation clock genes by analyzing the temporal expression profiles of the segmentation clock genes after establishing the circadian TTFL cycle. First, using our previous RNA-seq data from mouse fetal heart tissues before (E10–12) and after (E17–19) the emergence of circadian clock oscillation (*17*), we analyzed the temporal expression profiles of *Hes7* and *Lfng* (**Fig. 5A**). In both *Hes7* and *Lfng*, the temporal expression patterns at E17–19 tended to fluctuate with circadian fashion, in contrast to the absence of circadian rhythm at E10–12 (**Fig. 5A**). Furthermore, the expression of *Hes7* exhibited the oscillation with a circadian period in 28-day differentiated $Per2^{Luc}$ ESCs (*29*) and human epidermal stem cells (*30*) (**Fig. 5B, C**), both of which have functional circadian

clocks. Taking the previous reports which mentioned *Hes7* as a gene showing circadian fluctuation in various human and mouse tissues or cells into account (*31*), these results support that expression of the segmentation clock components *Hes7* and *Lfng* are likely to be entrained under circadian clock regulation after the establishment of circadian molecular oscillation. Because the loss of the *Hes7* ultradian expression rhythm and the genetic ablation or overexpression of *Lfng* in the mouse cause segmentation defects (*22, 32, 33*), oscillatory expressions of *Hes7* and *Lfng* genes with adequate ultradian rhythm are essential for mammalian development. Therefore, the results in this study suggest that it is imperative that the circadian clock oscillation is suppressed until the completion of segmentation and other related developmental events (**Fig. 5D**).

In summary, we have shown that premature excess of CLOCK/BMAL1 severely interferes with the ultradian rhythm of segmentation clock in iPSM and gastruloids, which highlights that the strict suppression of circadian clock oscillation during early to mid-developmental stage is essential for the intact process of mammalian embryogenesis. Interestingly, it was reported that hundreds of genes including *Per1* also oscillates in the same phase as *Hes7* in *in vitro*-PSM of both mouse and humans (*34*), suggesting that the segmentation clock-inducing ultradian rhythm entrains the expression in wide variety of genes in PSM. Gathering the evidence that circadian clock entrains *Hes7* and/or *Lfng* expression exhibiting daily fluctuation after the completion of circadian clock formation, the two distinct oscillators—the circadian clock and the segmentation clock—potentially interfere with each other. Altogether, the mutual exclusivity and rhythm conversion of the two different types of rhythm at the adequate timing reflect the indispensable biological significance of the "management of biological rhythms" in the developmental process in mammals.

References:

1. A. Balsalobre, F. Damiola, U. Schibler, A serum shock induces circadian gene expression in mammalian tissue culture cells. *Cell* **93**, 929-937 (1998).

2. J. S. Takahashi, Transcriptional architecture of the mammalian circadian clock. *Nat Rev Genet* **18**, 164-179 (2017).

3. K. Yagita, F. Tamanini, G. T. van Der Horst, H. Okamura, Molecular mechanisms of the biological clock in cultured fibroblasts. *Science* **292**, 278-281 (2001).

4. S. Yamazaki *et al.*, Resetting central and peripheral circadian oscillators in transgenic rats. *Science* **288**, 682-685 (2000).

5. S. H. Yoo *et al.*, PERIOD2::LUCIFERASE real-time reporting of circadian dynamics reveals persistent circadian oscillations in mouse peripheral tissues. *Proc Natl Acad Sci U S A* **101**, 5339-5346 (2004).

6. J. B. Hogenesch, H. R. Ueda, Understanding systems-level properties: timely stories from the study of clocks. *Nat Rev Genet* **12**, 407-416 (2011).

7. K. Yagita *et al.*, Development of the circadian oscillator during differentiation of mouse embryonic stem cells in vitro. *Proc Natl Acad Sci U S A* **107**, 3846-3851 (2010).

8. J. D. Alvarez, D. Chen, E. Storer, A. Sehgal, Non-cyclic and developmental stage-specific expression of circadian clock proteins during murine spermatogenesis. *Biol Reprod* **69**, 81-91 (2003).

9. T. Amano *et al.*, Expression and functional analyses of circadian genes in mouse oocytes and preimplantation embryos: Cry1 is involved in the meiotic process independently of circadian clock regulation. *Biol Reprod* **80**, 473-483 (2009).

10. E. Kowalska, E. Moriggi, C. Bauer, C. Dibner, S. A. Brown, The circadian clock starts ticking at a developmentally early stage. *J Biol Rhythms* **25**, 442-449 (2010).

11. D. Morse, N. Cermakian, S. Brancorsini, M. Parvinen, P. Sassone-Corsi, No circadian rhythms in testis: Period1 expression is clock independent and developmentally regulated in the mouse. *Mol Endocrinol* **17**, 141-151 (2003).

12. F. C. Davis, R. A. Gorski, Development of hamster circadian rhythms: role of the maternal suprachiasmatic nucleus. *J Comp Physiol A* **162**, 601-610 (1988).

13. C. Jud, U. Albrecht, Circadian rhythms in murine pups develop in absence of a functional maternal circadian clock. *J Biol Rhythms* **21**, 149-154 (2006).

14. S. M. Reppert, W. J. Schwartz, Maternal suprachiasmatic nuclei are necessary for maternal coordination of the developing circadian system. *J Neurosci* **6**, 2724-2729 (1986).

15. V. Carmona-Alcocer *et al.*, Ontogeny of Circadian Rhythms and Synchrony in the Suprachiasmatic Nucleus. *J Neurosci* **38**, 1326-1334 (2018).

16. Y. Umemura *et al.*, Transcriptional program of Kpna2/Importin-alpha2 regulates cellular differentiation-coupled circadian clock development in mammalian cells. *Proc Natl Acad Sci U S A* **111**, E5039-5048 (2014).

17. Y. Umemura *et al.*, Involvement of posttranscriptional regulation of Clock in the emergence of circadian clock oscillation during mouse development. *Proc Natl Acad Sci U S A* **114**, E7479-E7488 (2017).

18. Y. Umemura, I. Maki, Y. Tsuchiya, N. Koike, K. Yagita, Human Circadian Molecular Oscillation Development Using Induced Pluripotent Stem Cells. *J Biol Rhythms*, 748730419865436 (2019).

19. Y. Harima, I. Imayoshi, H. Shimojo, T. Kobayashi, R. Kageyama, The roles and mechanism of ultradian oscillatory expression of the mouse Hes genes. *Semin Cell Dev Biol* **34**, 85-90 (2014).

20. A. Hubaud, O. Pourquie, Signalling dynamics in vertebrate segmentation. *Nat Rev Mol Cell Biol* **15**, 709-721 (2014).

21. Y. Bessho, H. Hirata, Y. Masamizu, R. Kageyama, Periodic repression by the bHLH factor Hes7 is an essential mechanism for the somite segmentation clock. *Genes Dev* **17**, 1451-1456 (2003).

22. Y. Takashima, T. Ohtsuka, A. Gonzalez, H. Miyachi, R. Kageyama, Intronic delay is essential for oscillatory expression in the segmentation clock. *Proc Natl Acad Sci U S A* **108**, 3300-3305 (2011).

23. Y. Bessho *et al.*, Dynamic expression and essential functions of Hes7 in somite segmentation. *Genes Dev* **15**, 2642-2647 (2001).

24. M. Matsumiya, T. Tomita, K. Yoshioka-Kobayashi, A. Isomura, R. Kageyama, ES cell-derived presomitic mesoderm-like tissues for analysis of synchronized oscillations in the segmentation clock. *Development* **145**, (2018).

25. Y. B. Kiyohara *et al.*, The BMAL1 C terminus regulates the circadian transcription feedback loop. *Proc Natl Acad Sci U S A* **103**, 10074-10079 (2006).

26. S. C. van den Brink *et al.*, Single-cell and spatial transcriptomics reveal somitogenesis in gastruloids. *Nature* **582**, 405-409 (2020).

27. M. Kanehisa, S. Goto, KEGG: kyoto encyclopedia of genes and genomes. *Nucleic Acids Res* **28**, 27-30 (2000).

28. M. Ebisuya, T. Yamamoto, M. Nakajima, E. Nishida, Ripples from neighbouring transcription. *Nat Cell Biol* **10**, 1106-1113 (2008).

29. R. Ikeda *et al.*, REV-ERBalpha and REV-ERBbeta function as key factors regulating Mammalian Circadian Output. *Sci Rep* **9**, 10171 (2019).

30. P. Janich *et al.*, Human epidermal stem cell function is regulated by circadian oscillations. *Cell Stem Cell* **13**, 745-753 (2013).

31. X. Li *et al.*, CirGRDB: a database for the genome-wide deciphering circadian genes and regulators. *Nucleic Acids Res* **46**, D64-D70 (2018).

32. Y. Niwa *et al.*, The initiation and propagation of Hes7 oscillation are cooperatively regulated by Fgf and notch signaling in the somite segmentation clock. *Dev Cell* **13**, 298-304 (2007).

33. K. Serth, K. Schuster-Gossler, R. Cordes, A. Gossler, Transcriptional oscillation of lunatic fringe is essential for somitogenesis. *Genes Dev* **17**, 912-925 (2003).

34. M. Matsuda *et al.*, Recapitulating the human segmentation clock with pluripotent stem cells. *Nature* **580**, 124-129 (2020).

35. R. Yang, Z. Su, Analyzing circadian expression data by harmonic regression based on autoregressive spectral estimation. *Bioinformatics* **26**, i168-174 (2010).

36. Z. Chen *et al.*, Identification of diverse modulators of central and peripheral circadian clocks by high-throughput chemical screening. *Proc Natl Acad Sci U S A* **109**, 101-106 (2012).

37. Y. Inada *et al.*, Cell and tissue-autonomous development of the circadian clock in mouse embryos. *FEBS Lett* **588**, 459-465 (2014).

38. C. A. Schneider, W. S. Rasband, K. W. Eliceiri, NIH Image to ImageJ: 25 years of image analysis. *Nat Methods* **9**, 671-675 (2012).

39. H. M. T. Choi *et al.*, Third-generation in situ hybridization chain reaction: multiplexed, quantitative, sensitive, versatile, robust. *Development* **145**, (2018).

40. A. M. Bolger, M. Lohse, B. Usadel, Trimmomatic: a flexible trimmer for Illumina sequence data. *Bioinformatics* **30**, 2114-2120 (2014).

41. N. R. Coordinators, Database resources of the National Center for Biotechnology Information. *Nucleic Acids Res* **46**, D8-D13 (2018).

42. A. Dobin *et al.*, STAR: ultrafast universal RNA-seq aligner. *Bioinformatics* **29**, 15-21 (2013).

43. H. Li *et al.*, The Sequence Alignment/Map format and SAMtools. *Bioinformatics* **25**, 2078-2079 (2009).

44. A. Frankish *et al.*, GENCODE reference annotation for the human and mouse genomes. *Nucleic Acids Res* **47**, D766-D773 (2019).

45. S. Heinz *et al.*, Simple combinations of lineage-determining transcription factors prime cis-regulatory elements required for macrophage and B cell identities. *Mol Cell* **38**, 576-589 (2010).

46. M. I. Love, W. Huber, S. Anders, Moderated estimation of fold change and dispersion for RNA-seq data with DESeq2. *Genome Biol.* **15**, 550 (2014).

47. Y. Liao, J. Wang, E. J. Jaehnig, Z. Shi, B. Zhang, WebGestalt 2019: gene set analysis toolkit with revamped UIs and APIs. *Nucleic Acids Res* **47**, W199-W205 (2019).

48. H. Yoshitane *et al.*, Roles of CLOCK phosphorylation in suppression of E-box-dependent transcription. *Mol Cell Biol* **29**, 3675-3686 (2009).

Acknowledgments: We thank Yagita lab members for technical assistance; **Funding**: This work was supported in part by grants-in-aid for scientific research from the Japan Society for the Promotion of Science to Y.U. (19K06679) and K.Y. (18H02600), the Cooperative Research Program (Joint Usage/Research Center program) of Institute for Frontier Life and Medical Sciences, Kyoto University (K.Y. and G.K.); **Author contributions**: Y.U. and K.Y. designed the research; Y.U., Y.T., H.W., G.K., and K.Y. performed the research; Y.U., N.K., Y.T., R.K., and K.Y. analyzed the data; Y.U., N.K., and K.Y. wrote the paper; **Competing interests**: The authors declare no competing financial interests; **Data and materials availability**: All data are available in the main text and supplementary materials.

Supplementary Materials:

Materials and Methods

Figures S1–S5

References (*36–48*)

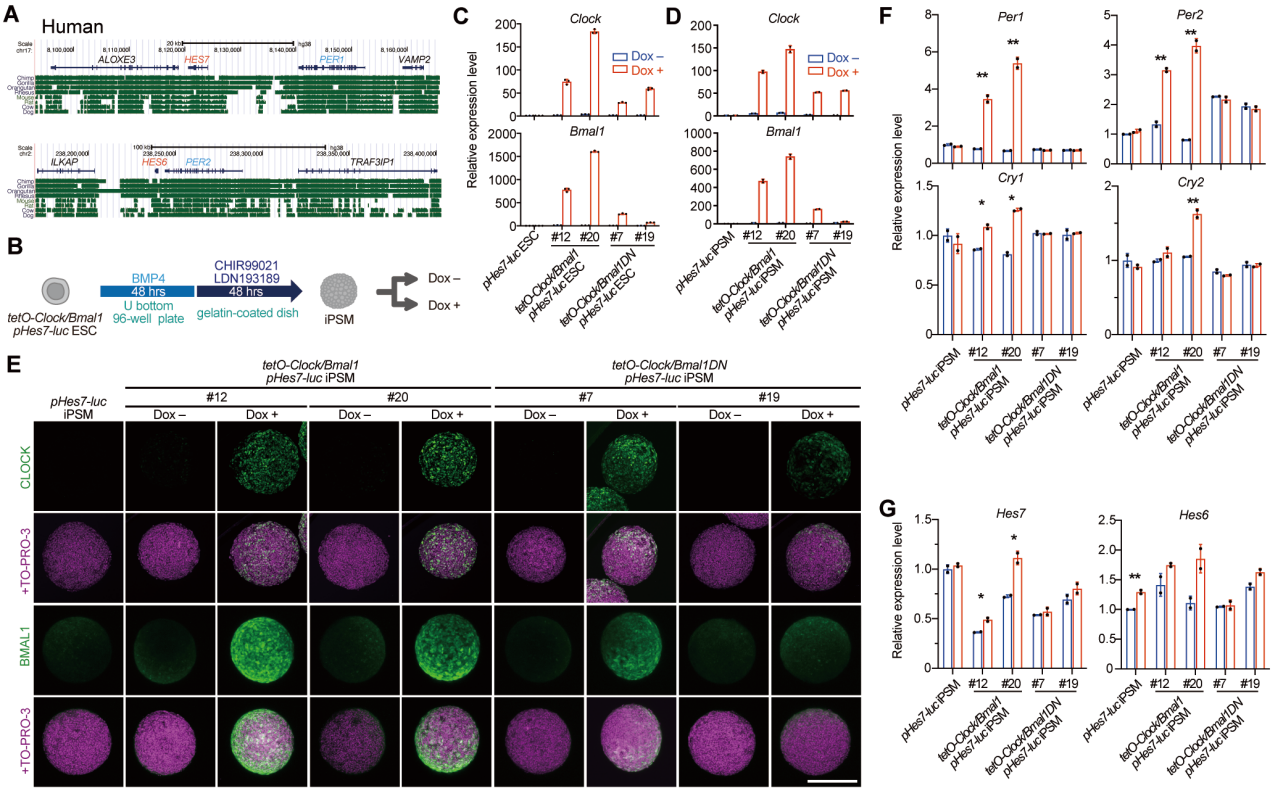

Fig. 1. CLOCK/BMAL1 expressions upregulated not only circadian clock genes but also *Hes7* gene expressions in iPSM. (**A**) Human genomic locus of circadian clock genes, *PER1*, and the essential segmentation clock gene, *HES7*, are highly conserved in higher vertebrates. The *PER1* homolog *PER2* is also located adjacent to the *HES7* homolog *HES6* in the genome. (**B**) ESCs were differentiated into iPSM for 96 h *in vitro*, and then the iPSM colonies were treated with or without dox. (**C**) qPCR of *Clock* and *Bmal1* mRNA in the indicated ESCs. 500 ng/mL dox treatment for 6 h (red) or not (blue). Each number indicates clone number. Mean ± SD (n = 3 biological replicates). (**D**) qPCR of *Clock* and *Bmal1* mRNA in the indicated iPSM colonies. 1000 ng/mL dox treatment for 2 h (red) or not (blue). Mean ± SD (n = 2 technical replicates). (**E**) Representative maximum intensity projection of the immunostaining of iPSM colonies treated with 1000 ng/mL dox for 2 h or not. n = 2–3 biological replicates. Scale = 250 μm. (**F, G**) qPCR of core circadian clock gene (**F**) and *Hes7* or *Hes6* gene (**G**) in the indicated iPSM colonies. 1000 ng/mL dox treatment for 2 h (red) or not (blue). Mean ± SD (n = 2 technical replicates).

The average expression level of *pHes7-luc* ESCs or iPSM colonies without dox was set to 1. Two-tailed t-test, *P < 0.05, **P < 0.01.

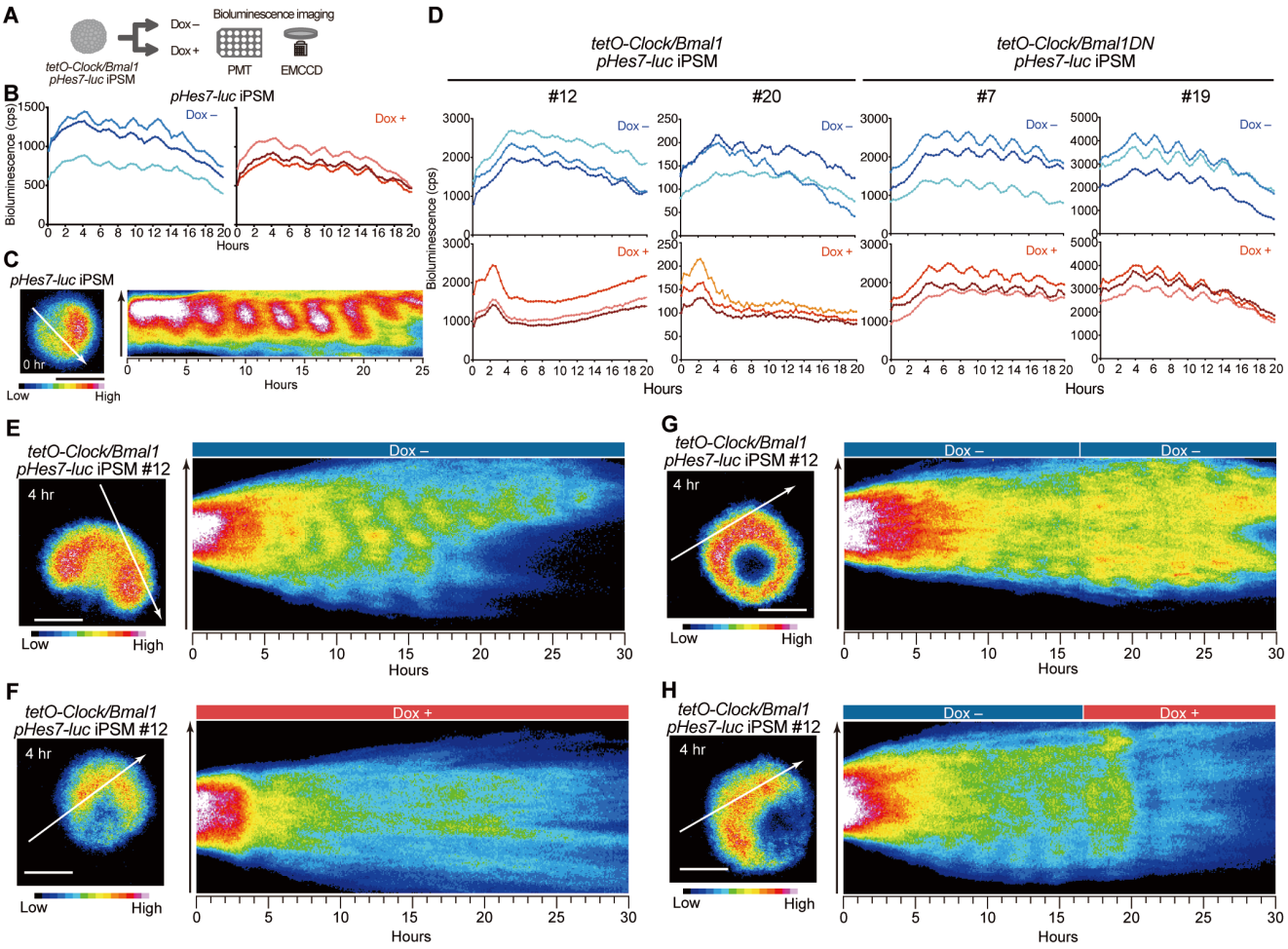

Fig. 2. CLOCK/BMAL1 expressions arrested the autonomous oscillations of *Hes7* in the iPSM colonies. (**A**) Bioluminescence of each dox-inducible *Clock/Bmal1* or *Clock/Bmal1DN* *pHes7-luc* iPSM colony was observed using PMT or an EM-CCD camera without or with dox. (**B, C**) Bioluminescence traces (**B**) and live imaging (**C**) of single *pHes7-luc* iPSM colony with or without dox. The kymograph of the imaging along the arrow is shown. (**D**) Bioluminescence traces of the single indicated iPSM colony with and without 1000 ng/mL dox. (**E–H**) Live imaging of the single *tetO-Clock/Bmal1 pHes7-luc* iPSM colony with and without dox. Dox-containing medium or only medium was added at the indicated time points at the final dox concentration of 1000 ng/mL (**G, H**). Each kymograph along the arrow is shown. Scales = 250 μm.

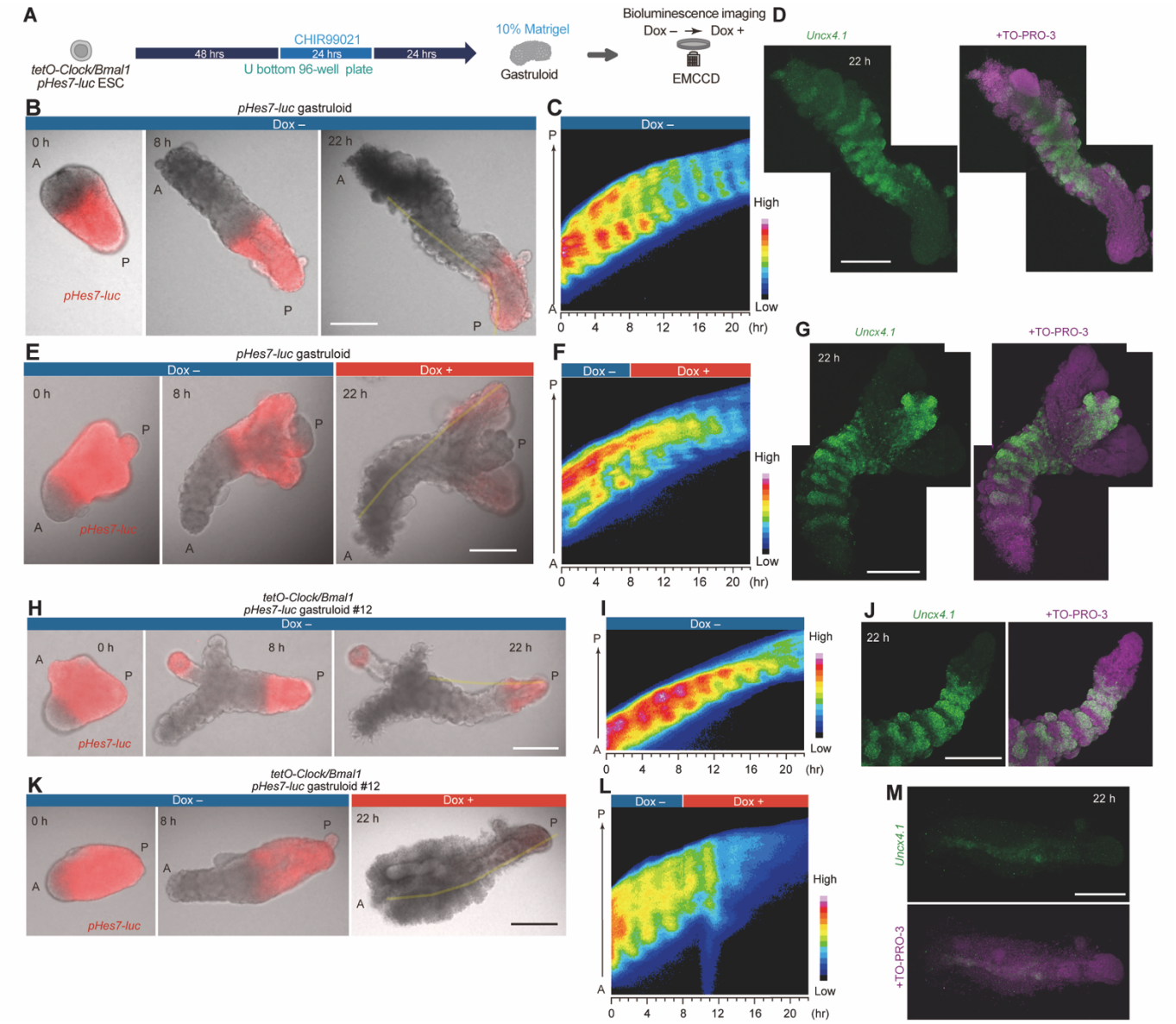

Fig. 3. CLOCK/BMAL1 expressions arrested the autonomous oscillations of *Hes7* and somitogenesis-like process in the gastruloids. (**A**) Dox-inducible *Clock/Bmal1 pHes7-luc* ESCs were differentiated into gastruloids for 96 h *in vitro*, and then the gastruloids embedded in 10% Matrigel were treated with or without dox. *pHes7-luc* bioluminescence was observed using an EM-CCD camera without or with dox. (**B–M**) Time-lapse bioluminescence (red) and bright field imaging of the single *pHes7-luc* gastruloid or *tetO-Clock/Bmal1 pHes7-luc* gastruloid without and with dox. Dox-containing medium was added at the indicated time points at the final dox concentration of 1000 ng/mL (**C, F, I, L**). Each kymograph is shown along the yellow lines in **B,**

E, H, K. *In situ* hybridization of *Uncx4.1* in the gastruloids after the live cell imaging (**D, G, J, M**). Scales = 250 μm.

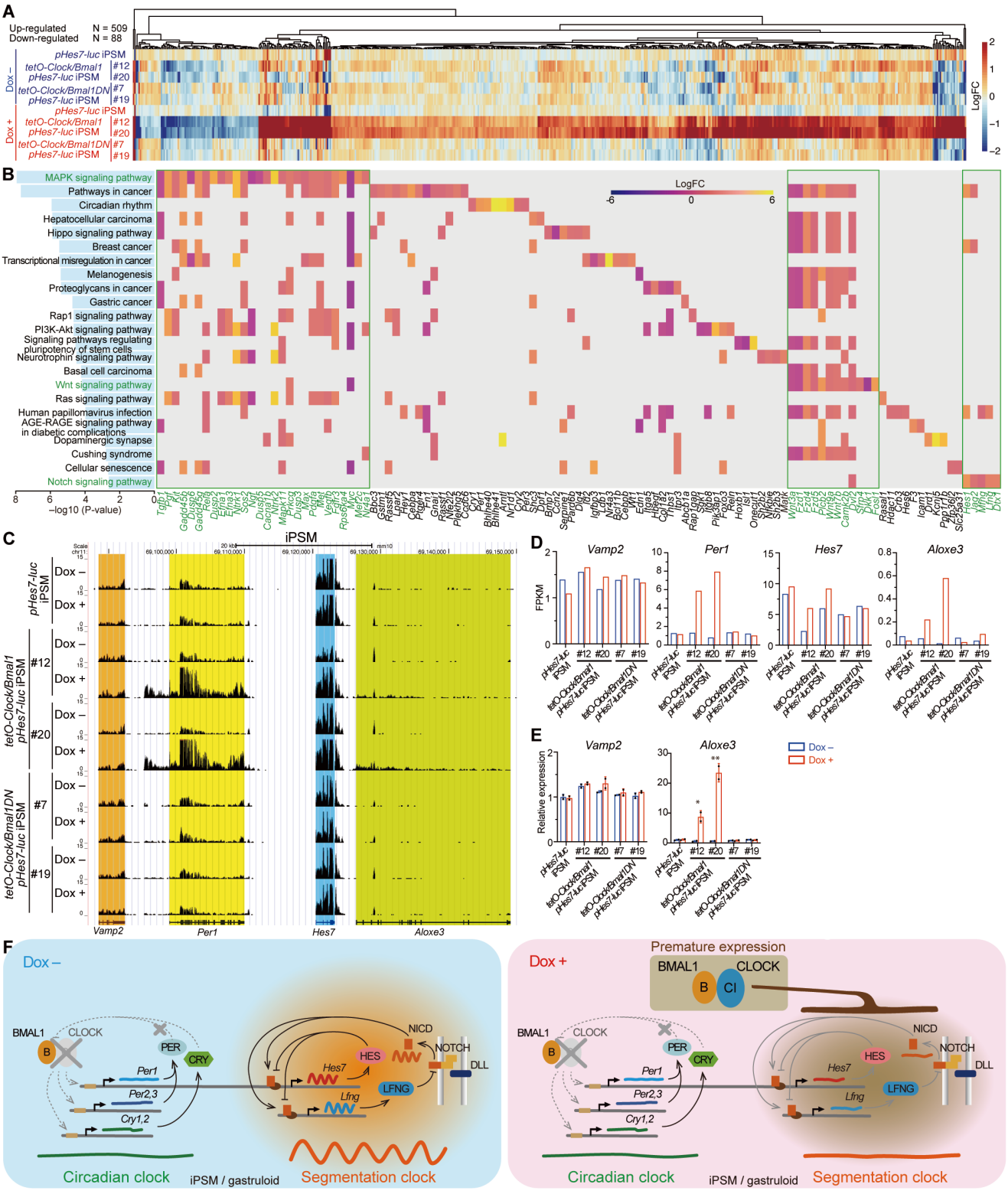

Fig. 4. CLOCK/BMAL1 expressions in the iPSM colonies affected *Hes7*-related signaling pathways and upregulated the expression of contiguous genes, *Per1*, *Hes7*, and *Aloxe3*. (A)

Upregulated and downregulated DEGs in the indicated iPSM colonies treated with dox. (**B**) KEGG pathway analysis of the DEGs. Each pathway was indicated with each transformed p-value. The ranked pathways contained several common genes in the WNT, MAPK, and NOTCH signaling pathways. (**C**) UCSC genome browser views of RNA-seq data of the contiguous genes *Vamp2*, *Per1*, *Hes7*, and *Aloxe3*. The reads shown are normalized average reads per 10 million total reads in 10-bp bins. (**D**) mRNA expression of *Vamp2*, *Per1*, *Hes7*, and *Aloxe3* in the indicated iPSM colonies according to RNA-seq. (**E**) Validation of *Vamp2* and *Aloxe3* gene expression levels in the indicated iPSM colonies using qPCR. Colored boxes indicate 1000 ng/mL dox treatment for 2 h (red) or no treatment (blue). Mean ± SD (n = 2 technical replicates). The averaged expression level of *pHes7-luc* iPSM colonies without dox was set to 1. Two-tailed t-test, *P < 0.05, **P < 0.01. (**F**) The premature expression of CLOCK/BMAL1 in the iPSM and gastruloids interfered with the segmentation clock oscillation and somitogenesis-like process, suggesting that it is necessary to suppress the circadian clock oscillation until the completion of segmentation.

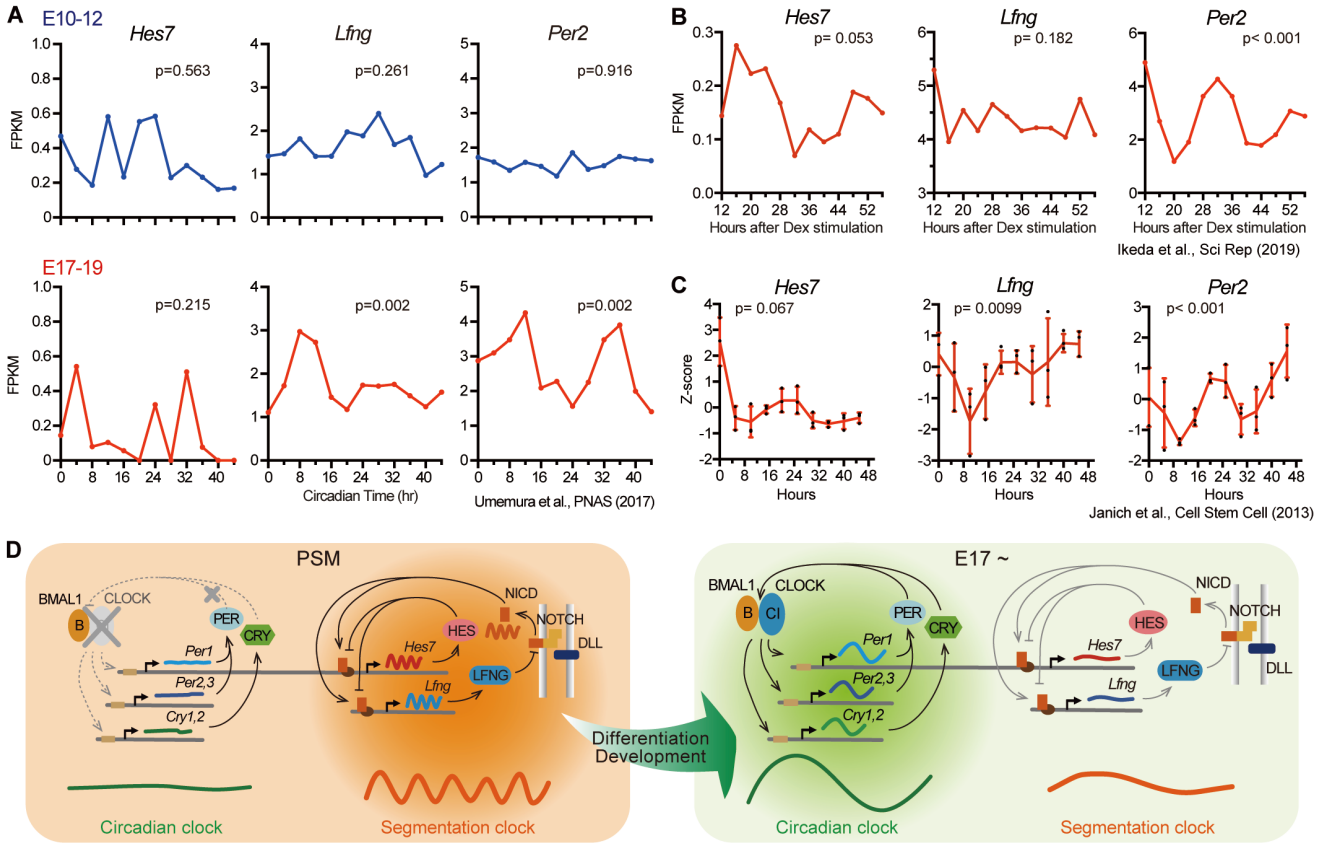

Fig. 5. Gene expression profiles of *Hes7*, *Lfng*, and *Per2*. (A) *Hes7*, *Lfng*, and *Per2* gene expression levels measured using RNA-seq in fetal mouse hearts at E10–12 or E17–19 (DRA005754) (*17*). (**B, C**) *Hes7*, *Lfng*, and *Per2* gene expressions in *in vitro* 28-day differentiated *Per2*^{Luc} ESCs (**B**, GSE125696) and in human epidermal stem cells (**C**, GSE50631). The P values of circadian rhythmicity were calculated by ARSER (*35*). The mean expression values from the replicates were used to determine cycling for human microarray data. (**D**) After the completion of somitogenesis, the circadian clock is established and the systematic circadian rhythm regulation may fluctuate the components of the segmentation clock with a circadian period.

Supplementary Materials for

CLOCK/BMAL1 interferes with segmentation clock oscillation in mouse embryonic organoids

Yasuhiro Umemura, Nobuya Koike, Yoshiki Tsuchiya, Hitomi Watanabe, Gen Kondoh, Ryoichiro Kageyama, and Kazuhiro Yagita

Correspondence to: kyagita@koto.kpu-m.ac.jp

This PDF file includes:

Materials and Methods

Figs. S1 to S5

Materials and Methods

Cell culture

KY1.1 ESCs (*7*), referred to as ESC in the text, and *Per2*^{Luc} ESCs (*5, 36*) were maintained as described previously (*17*). E14TG2a ESCs carrying *Hes7*-promoter-driven luciferase reporters (*24*), referred to as *pHes7-luc* ESCs, were maintained without feeder cells in DMEM (Nacalai) supplemented with 15% fetal bovine serum (Hyclone), 2 mM L-glutamine (Nacalai), 1 mM nonessential amino acids (Nacalai), 100 μM StemSure® 2-mercaptoethanol solution (Wako), 1 mM sodium pyruvate (Nacalai), 100 units/mL penicillin and streptomycin (Nacalai), 1000

units/mL leukemia inhibitory factor (Wako), 3 μM CHIRON99021 (Wako), and 1 μM PD0325901 (Wako) with 5% CO_2 at 37°C.

Transfection and establishment of cell lines

ESCs stably expressing dox-inducible *Clock/Bmal1* or *Clock/Bmal1DN* (I584X) were established as described previously (*17*). For *TetO-Clock/Bmal1* or *TetO-Clock/Bmal1DN* ESCs, KY1.1 ESCs or *pHes7-luc* ESCs were transfected using 10.5 μl of FuGENE 6 mixed with 1 μg of pCAG-PBase, 1 μg of PB-TET-Clock (*17*), 1 μg of PB-TET-Bmal1 or PB-TET-Bmal1DN (I584X), 1 μg of PB-CAG-rtTA Adv, and 0.5 μg of puromycin selection vector. The transfected cells were grown in a culture medium supplemented with 2 μg/mL puromycin for 2 days. The ESC colonies were picked and checked by qPCR after treatment with 500 ng/mL doxycycline. For PB-TET-Bmal1 and PB-TET-Bmal1DN (I584X), Bmal1 cDNA and Bmal1DN (I584X) cDNA (*25*) were cloned into a PB-TET vector (*37*). For the *TetO-Clock Per2*^{Luc} ESCs, *Per2*^{Luc} ESCs were established as described previously (*17*).

Bioluminescence imaging

The iPSM colonies were differentiated from the *pHes7-luc* ESCs as described previously (*24*). Bioluminescence imaging of single iPSM colonies was performed in gelatin-coated 24-well black plates (*25*). DMEM was used that was supplemented with 15% Knock-out Serum Replacement (KSR), 2 mM L-glutamine, 1 mM nonessential amino acids, 1 mM sodium pyruvate, 100 units/mL penicillin and streptomycin, 0.5% DMSO, 1 μM CHIRON99021, and 0.1 μM LDN193189 (Sigma) containing 1 mM luciferin and 10 mM HEPES. For live imaging of single iPSM colonies using an EM-CCD camera, each iPSM colony was cultured on a fibronectin-coated glass base dish for 6 h, and images were acquired every 5 min with an

exposure time of 10 s (control) or 2.5 s (*Clock/Bmal1* induction) under 5% CO_2 using an LV200 Bioluminescence Imaging System (Olympus).

Gastruloids were generated as described in a previous report (*26*). In total, 200–250 live cells were plated in 40 µl of N2B27 medium into each well of a U-bottomed nontissue culture-treated 96-well plate (Greinier 650185). After 96-h cultivation, the gastruloids were embedded in 10% Matrigel (Corning 356231) containing 1 mM luciferin. For live imaging of single gastruloids, the images were acquired every 5 min with an exposure time of 3.5 s (*Clock/Bmal1* induction) or 10 s (control) under 5% CO_2 using the LV200 system. The movies were analyzed using the ImageJ 1.53e software (*38*). Kymographs of the averaged bioluminescence intensity along the straight or segmented line of 5-pixel width were generated using the plug-in KymoResliceWide.

In situ hybridization

Hybridization chain reaction (HCR) V3 was performed as described previously (*26, 39*) using reagents procured from Molecular Instruments. *Uncx4.1* HCR probe (Accession NM_013702.3, hairpin B1) was labeled with Alexa Fluor 488.

Quantitative RT-PCR

iPSM colonies, ESCs, and gastruloids were washed with ice-cold PBS, and total RNA was extracted using Isogen reagent (Nippon Gene) or miRNeasy Mini Kits (QIAGEN) according to the manufacturer's instructions. To remove the feeder cells from ESCs cultured on a feeder layer, the cells were treated with trypsin, and then the mixed cell populations were seeded on gelatin-coated dishes and incubated for 25 min at 37°C 3 times in ES cell medium. Nonattached ESCs were seeded in a gelatin-coated dish overnight and then treated with or without 500 ng/mL

doxycycline for 6 h. iPSM colonies and gastruloids were treated with or without 1000 ng/mL doxycycline for 2 h. First-strand cDNAs were synthesized with 1000 or 280 ng of total RNA using M-MLV reverse transcriptase (Invitrogen) according to the manufacturer's instructions. Quantitative PCR analysis was performed using the StepOnePlus™ Real-Time PCR system (Applied Biosystems) and iTaq™ Universal SYBR Green Supermix (Bio-Rad Laboratories). Standard PCR amplification protocols were applied, followed by dissociation-curve analysis to confirm specificity. Transcription levels were normalized to the level of β-actin. The following primer sequences were used:

Bmal1	Forward (F)	CCACCTCAGAGCCATTGATACA
Bmal1	Reverse (R)	GAGCAGGTTTAGTTCCACTTTGTCT
Clock	F	ATTTCAGCGTTCCCATTTGA
Clock	R	TGCCAACAAATTTACCTCCAG
Per1	F	CCCAGCTTTACCTGCAGAAG
Per1	R	ATGGTCGAAAGGAAGCCTCT
Per2	F	CAGCACGCTGGCAACCTTGAAGTAT
Per2	R	CAGGGCTGGCTCTCACTGGACATTA
Cry1	F	TGAGGCAAGCAGACTGAATATTG
Cry1	R	CCTCTGTACCGGGAAAGCTG
Cry2	F	CTGGCGAGAAGGTAGAGTGG
Cry2	R	GACGCAGAATTAGCCTTTGC
Dbp	F	CGAAGAACGTCATGATGCAG
Dbp	R	GGTTCCCCAACATGCTAAGA
Hes6	F	CAACGAGAGTCTTCAGGAGCTGCG
Hes6	R	GCATGCACTGGATGTAGCCAGCAG

Hes7	F	GAGAGGACCAGGGACCAGA
Hes7	R	TTCGCTCCCTCAAGTAGCC
Vamp2	F	GAGCTGGATGACCGTGCAGATG
Vamp2	R	ATGGCGCAGATCACTCCCAAGA
Aloxe3	F	AAGCCCGCCAAGAATGTTATC
Aloxe3	R	CGGTTCCCAGAGTTGTCATCC
Actb	F	GGCTGTATTCCCCTCCATCG
Actb	R	CCAGTTGGTAACAATGCCATGT

RNA-seq

The iPSM colonies and ESCs were washed with ice-cold PBS, and total RNA was extracted using miRNeasy Mini Kits (QIAGEN) according to the manufacturer's instructions. Total RNA sequencing was conducted by Macrogen Japan on an Illumina NovaSeq 6000 with 101-bp paired-end reads. After trimming the adaptor sequences using Trimmomatic (*40*), the reads that mapped to ribosomal DNA (GenBank: BK000964.1) (*41*) were filtered out and the sequence reads were mapped to the mouse genome (GRCm38/mm10) using STAR (*42*), as described previously (*16*). To obtain reliable alignments, reads with a mapping quality of less than ten were removed using SAM tools (*43*). The known canonical genes from GENCODE VM23 (*44*) were used for annotation, and the reads mapped to the gene bodies were quantified using Homer (*45*). The longest transcript for each gene was used for gene-level analysis. We assumed that a gene was expressed when there were more than 20 reads mapped on average to the gene body. Differential gene expression in the RNA-seq data was determined using DESeq2 with thresholds of FDR < 0.05, fold change > 1.5, and expression level cutoff > 0.01 FPKM (*46*). WebGestalt was used for KEGG pathway enrichment analysis (*47*). In the RNA-seq data using iPSM

colonies, the reads mapped in the promoter (chr11:69115096-69120473) and 3′UTR (chr11:69122995-69123324) of *Hes7* were filtered out to eliminate transcripts from the *pHes7-luc* reporter transgene. The heatmaps of gene expression and KEGG pathways were generated with R using the pheatmap and pathview packages, respectively.

Immunostaining

The iPSM colonies were fixed in cold methanol for 15 min at room temperature. The fixed iPSM was blocked with 1% BSA and then incubated with anti-CLOCK antibody (CLSP4) (*48*) or anti-BMAL1 (MBL, JAPAN) overnight at 4°C. After washing in 1% BSA, the iPSM colonies were incubated with a CF™488A-conjugated donkey anti-mouse IgG (Nacalai) for 2 h at 4°C, and the nuclei were stained with TO-PRO®-3 1:1000 (Thermo Fisher Scientific, USA) for 10–20 min. The iPSM colonies were washed in 1% BSA and observed using an LSM510 confocal laser scanning microscope (Zeiss).

Data availability

RNA sequence data are available at the Gene Expression Omnibus. All other datasets generated in this study are available from the corresponding author upon reasonable request.

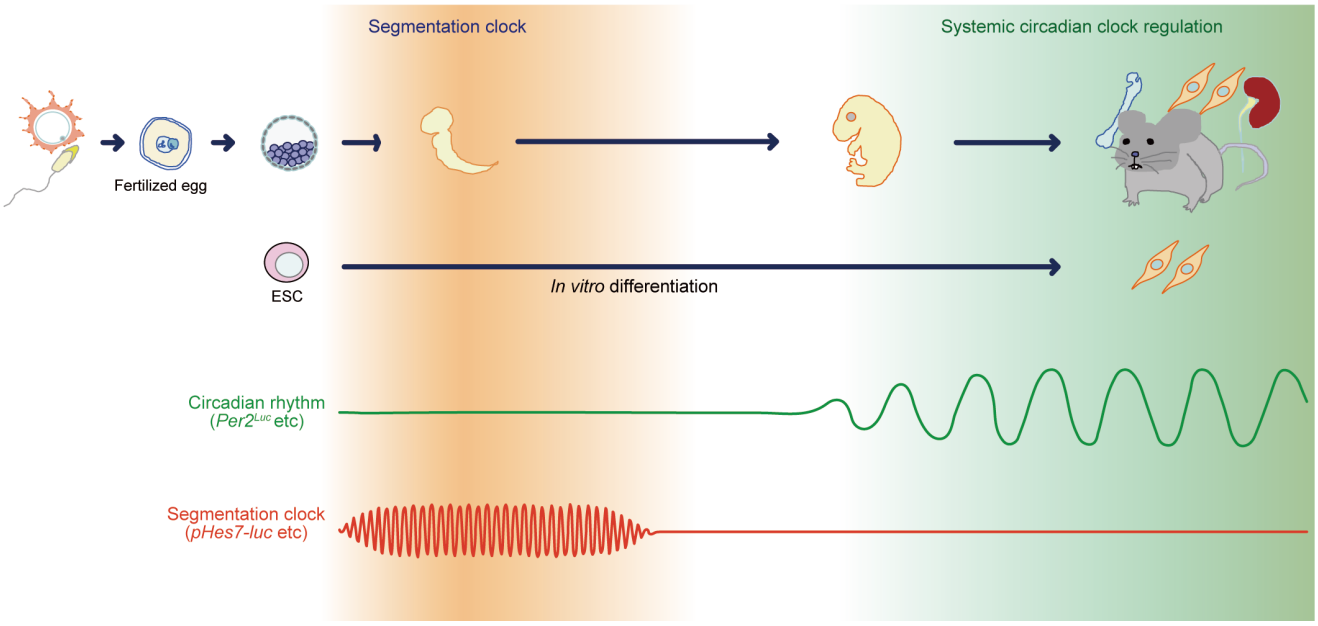

Fig. S1. Mutual exclusiveness of segmentation clock and circadian clock. In mammals, two different types of rhythm appear sequentially during the developmental process. One is the ultradian rhythm by segmentation clock, which controls somitogenesis. The other one is the circadian oscillation, which regulates the predictive adaptation of physiological functions to the day–night environmental cycle.

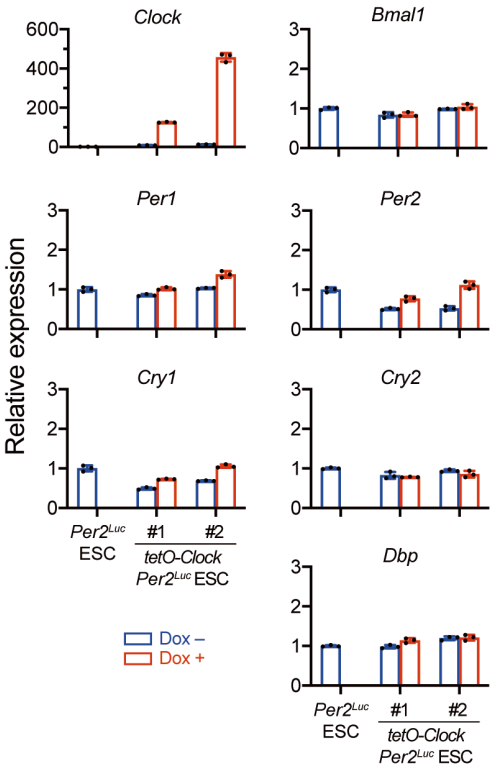

Fig. S2. The core circadian clock gene expressions in the ESCs harboring dox-inducible *Clock*. Although the expression of BMAL1 protein was observed even in ESCs (*17*), dox-dependent sole expression of *Clock* was insufficient for the E-box-driven expression of clock genes such as *Per1/2* and *Cry1/2* in undifferentiated ESCs, suggesting a possibility that the endogenously expressed BMAL1 is posttranslationally modified not to function. Colored boxes indicate 500 ng/mL dox treatment for 6 h (red) or no treatment (blue). Each number indicates clone number. Mean ± SD (n = 3 biological replicates). The averaged expression level of *Per2*^{Luc} ESCs without dox was set to 1.

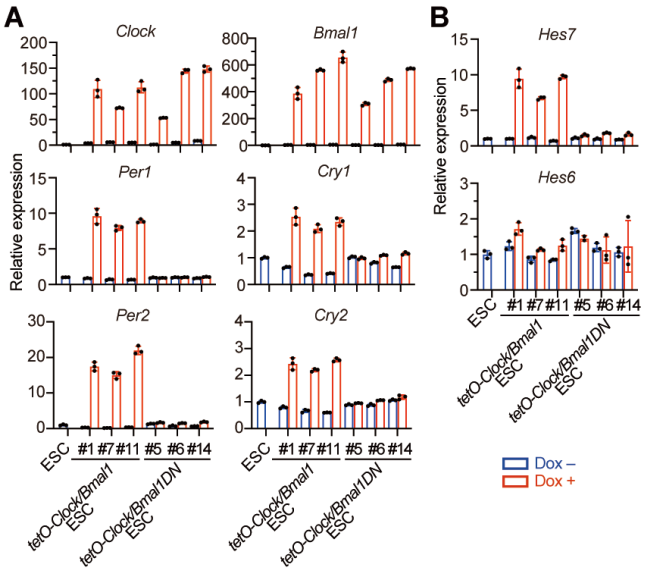

Fig. S3. *Clock/Bmal1* gene expressions in ESCs upregulated not only circadian clock genes but also *Hes7* gene expression. (**A, B**) qPCR of core circadian clock gene (**A**) and *Hes*7 or *Hes6* gene (**B**) expression in ESCs harboring dox-inducible *Clock* and *Bmal1* or *Clock* and *Bmal1DN*. Colored boxes indicate the presence (red) or absence (blue) of 500 ng/mL dox treatment for 6 h. Each number indicates clone number. Mean ± SD (n = 2–3 biological replicates). The average expression level of ESCs without dox was set to 1.

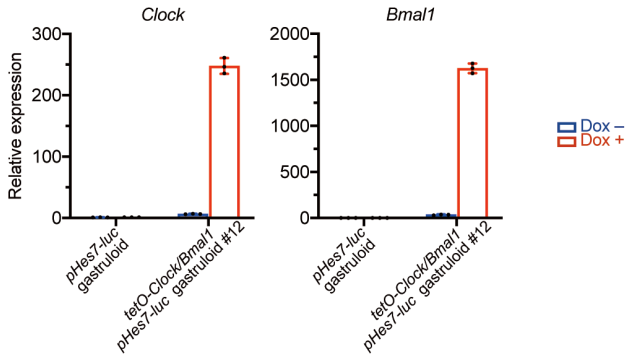

Fig. S4. qPCR of *Clock* and *Bmal1* mRNA in the indicated gastruloids. Colored boxes indicate 1000 ng/mL dox treatment for 2 h (red) or no treatment (blue). Each number indicates clone number. Mean ± SD (n = 3 biological replicates). The average expression level of *pHes7-luc* gastruloids without dox was set to 1.

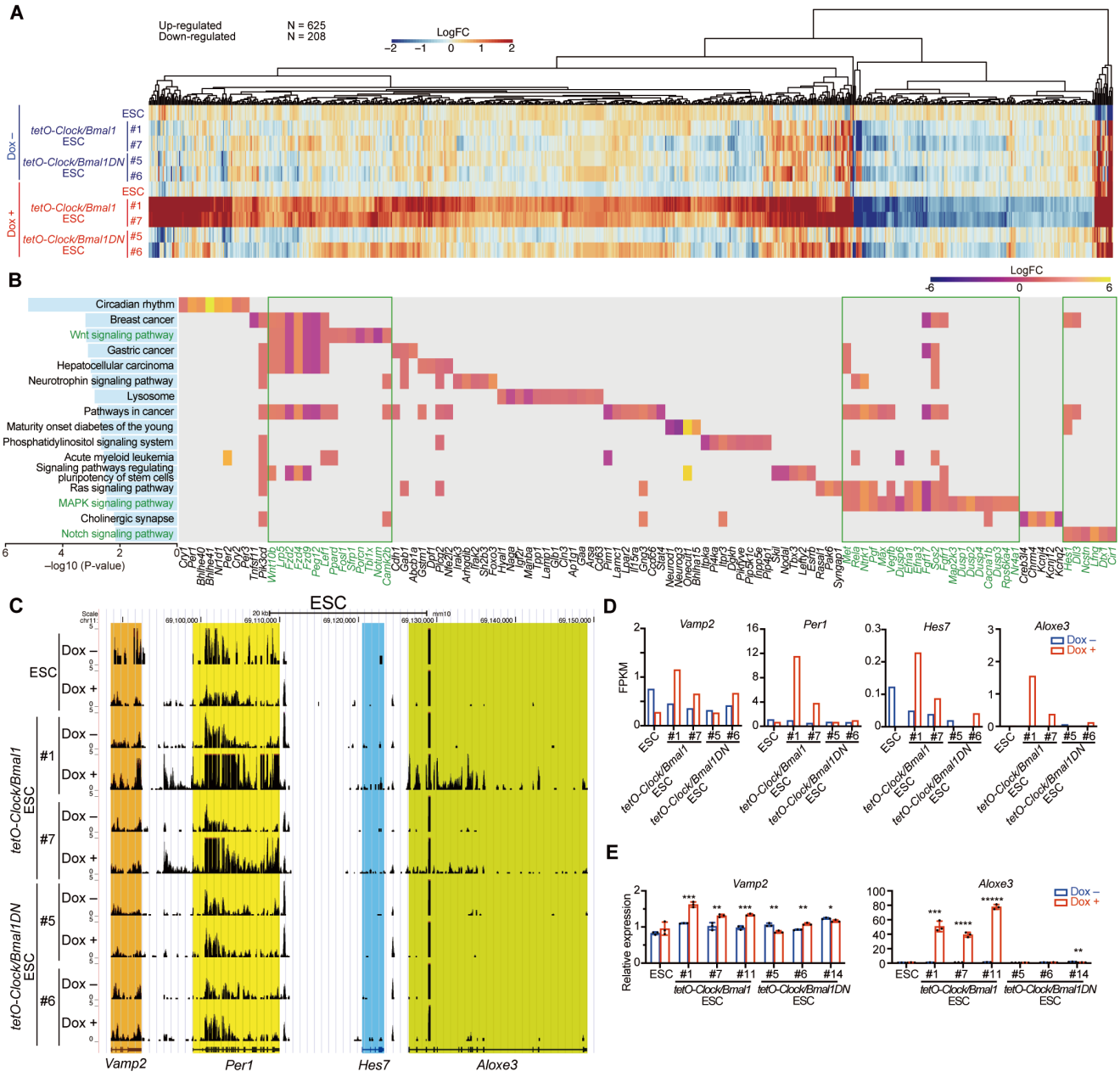

Fig. S5. ***Clock/Bmal1*** **gene expressions in ESCs affected the** ***Hes7*****-related signaling pathways and upregulated the expression of the contiguous genes** ***Vamp2, Per1*****,** ***Hes7*****, and** ***Aloxe3*****.** (**A**) Upregulated and downregulated differentially expressed genes in the indicated ESCs treated with dox (FDR < 0.05, FC > 1.5). (**B**) KEGG pathway analysis of the DEGs. Each pathway was indicated with each transformed p-value. The ranked pathways contained several common genes in the WNT, MAPK, and NOTCH signaling pathways. (**C**) UCSC genome

browser views of RNA-seq data of contiguous genes, including *Vamp2*, *Per1*, *Hes7*, and *Aloxe3*. The reads shown are normalized average reads per 10 million total reads in 10-bp bins. (**D**) mRNA expression of *Vamp2*, *Per1*, *Hes7*, and *Aloxe3* in the indicated ESCs measured using RNA-seq. (**E**) Validation of *Vamp2* and *Aloxe3* in the indicated ESCs by qPCR. Colored boxes indicate the use of 500 ng/mL dox treatment for 6 h (red) or untreated cells (blue). Each number indicates clone number. Mean ± SD (n = 3 biological replicates). Two-tailed t-test, *P < 0.05, **P < 0.01, ***P < 0.001, ****P < 0.0001, *****P < 0.00001